View Online / Journal Homepage / Table of Contents for this issue
Dynamic Article Links

Nanoscale

Cite this: *Nanoscale*, 2012, **4**, 2783

www.rsc.org/nanoscale

REVIEW

Recent advances in solar cells based on one-dimensional nanostructure arrays

Miao Yu,[a] Yun-Ze Long,*[bc] Bin Sun[b] and Zhiyong Fan*[a]

Received 24th February 2012, Accepted 13th March 2012
DOI: 10.1039/c2nr30437f

As the demand for renewable energy resource is growing rapidly worldwide, a variety of energy materials and technologies are being developed. In this review, we aim to summarize recent developments in the state-of-the-art research on energy harvesting technologies such as thin-film Si or Ge, CdTe, GaAs, organic, hybrid, and dye-sensitized solar cells (DSSCs) utilizing one-dimensional (1D) nanomaterials, mainly semiconductor nanowires, nanocones, nanotubes and nanofibers, which are prepared by vapor–liquid–solid method, colloidal lithography, template-guided growth, or electrospinning. Moreover, the future challenges (such as efficiency improvement and natural resource limitations) and prospects of nanostructured solar cells are proposed.

1 Introduction

According to the investigations of the U.S. energy information administration (EIA), the world energy demand in 2010 has reached 15 TW.[1] The predicted energy demand will reach 28 TW by 2050 and 46 TW by 2100.[2] However, about 80% of the present energy comes from fossil fuels. The increased concerns about the decreased availability of fossil fuel sources, the long-term environmental effects of CO_2, and the rapidly increasing energy demand in the future are driving enormous efforts for advanced renewable energy technologies. It is estimated that in 2040, more than 80% of the global electricity will be generated from renewable energy (as shown in Fig. 1).[3] Among various renewable energy technologies, solar photovoltaics that directly convert energy of sunlight into electricity have attracted a lot of interest both from scientific research and industrial production because of its abundance and cleanliness. However, at present solar photovoltaics only supply a very small portion of the global electricity consumption (<0.04%). Its contribution as estimated

[a]*Department of Electronic & Computer Engineering, Hong Kong University of Science & Technology (HKUST), Hong Kong SAR, China. E-mail: eezfan@ust.hk*
[b]*College of Physics Science, Qingdao University, Qingdao 266071, China. E-mail: yunze.long@163.com*
[c]*State Key Laboratory Cultivation Base of New Fiber Materials & Modern Textile, Qingdao University, Qingdao 266071, China*

Yun-Ze LONG

Yun-Ze Long received his BSc degree from the University of Science & Technology of China in 2000 and received a PhD degree from the Institute of Physics, Chinese Academy of Sciences in 2005. He then worked in the Institut des Materiaux Jean Rouxel, CNRS, France, as a postdoctoral fellow. He has been with the Qingdao University since Dec. 2006, where he is currently a full Professor. From 2009 to 2011, he worked as a visiting researcher in the University of Sydney and the HKUST. He has authored or coauthored more than 70 papers. He holds 9 Chinese patents. His research interests focus on one-dimensional functional nanomaterials.

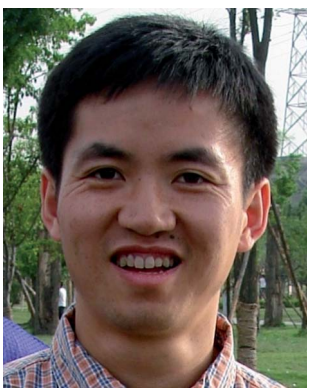

Zhiyong FAN

Zhiyong Fan received his BSc and MSc degree from Fudan University, China, in 1998 and 2001, respectively. He received a PhD degree from the University of California, Irvine in 2006. From 2007 to 2010, he worked in the University of California, Berkeley as a postdoctoral fellow, with a joint appointment with the Lawrence Berkeley National Laboratory. In May 2010, he joined the HKUST as an Assistant Professor. He has published more than 60 peer-reviewed papers with 2500 citations. He holds 2 Chinese and 1 US patents. His research effort concentrates on engineering novel nanostructures with functional materials, for technological applications including energy conversion, electronics and sensors.

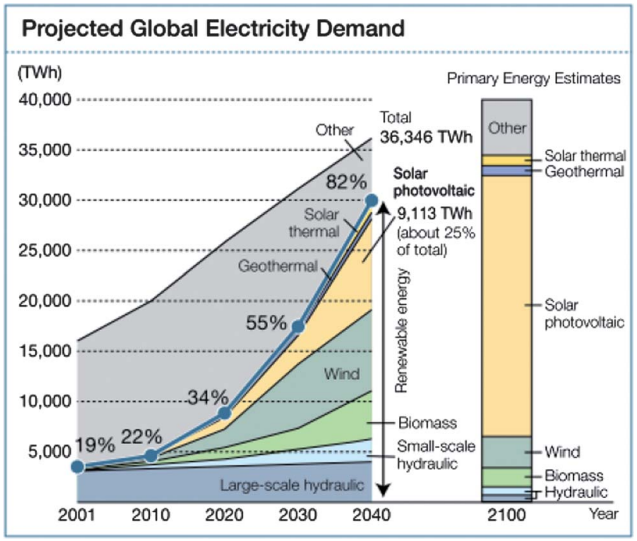

Fig. 1 Projected global electricity demand (Source: Created by Sharp based on *Renewable Energy Scenario to 2040*, published by the European Renewable Energy Council (EREC), and reports of the German Advisory Council on Global Change (WBGU)).

by the European Renewable Energy Council (EREC) will increase to about 25% in 2040 and more than 65% in 2100 (Fig. 1).

Currently, solar photovoltaic production is dominated by crystalline Si modules, the first generation of solar cells, which occupy about 90% of the photovoltaic market at present. In spite of a substantial drop in the cost over the past 50 years, terawatt-scale implementation of solar cells is currently not economically feasible because of the higher cost comparing with traditional power sources (as shown in Fig. 2).[4] However, it is estimated that the solar power cost will fall about 10 percent a year in the next decade as technology improves, while the expense of producing electricity by burning fossil fuels will climb gradually with oil and coal prices. The solar power cost may equal fossil fuel expenses within the next several years (Fig. 2). Therefore, it is still necessary and challenging to make significant technology improvement in both device performance and the manufacturing process

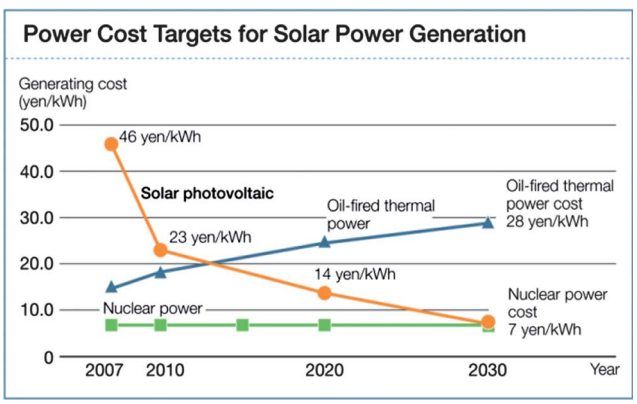

Fig. 2 Power cost targets for solar power, oil-fired thermal power and nuclear power generation (Source: Sharp based on *Photovoltaic Roadmap 2030*, published by the New Energy and Industrial Technology Development Organization (NEDO)).

so that solar cells could be economically competitive for large-scale applications.

The most important parameters for evaluating solar cells are efficiency and cost. As shown in Fig. 3,[5a] different kinds of materials have been symmetrically investigated over the past forty years, including crystalline Si, GaAs, and thin films such as CdTe, $CuIn_{1-x}Ga_xSe_2$ (CIGS) and hydrogenated amorphous Si (a-Si:H) with typical thickness of 1–2 μm, which were named as first and second generation solar cells, respectively. The first generation cells have high efficiency but are relatively expensive to produce. The second generation cells have lower efficiency, but the cost per watt is lower than that of the first generation cells. For the coming third generation or emerging photovoltaics, such as dye-sensitized, organic, inorganic and quantum dot cells, nanostructured solar cells are considered as one of the most promising technologies to achieve the goal of both high efficiency and low cost.[5b] Besides the material system, geometry and structure are key factors for high performance solar cells. In the past several years, different nanostructured (*e.g.*, quantum dots/nanoparticles, nanowires, nanopillars/rods, nanotubes/nanoholes, nanocones, nanofibers, nanotrees, and nanocomposites, *etc.*) photovoltaics including dye-sensitized cells, organic or hybrid organic-inorganic cells have been reported extensively,[6–12] which can usually reduce optical reflection, improve absorption or charge carrier collection efficiency.

In this paper, we aim to review recent developments in the state-of-the-art research on energy harvesting technologies such as thin-film Si or Ge, CdTe, GaAs, organic, hybrid, and dye-sensitized solar cells that utilize one-dimensional (1D) nanomaterials, mainly semiconductor nanowires, nanocones, nanotubes and nanofibers, which are prepared by chemical vapour deposition (CVD), colloidal lithography, template-guided deposition, or electrospinning. In addition, the future challenges (such as efficiency improvement and natural resource limitations) and prospects of nanostructured solar cells are proposed.

2 Fabrication of 1D nanostructure arrays

1D nanostructure arrays can be prepared by a variety of "bottom-up" and "top-down" approaches such as CVD, solution chemistry, photo- and electron-beam lithography, nanoimprinting, *etc.*[13–15] In this section, we briefly introduce several commonly used methods in nanostructured solar cells: the vapor–liquid–solid (VLS) method, colloidal lithography, template-guided deposition and electrospinning. These methods can fabricate 1D nanostrucutures on a large scale with relatively low cost and relative high throughout.

The VLS method is a catalytic vapor phase growth approach for the synthesis of 1D nanowire arrays from CVD.[13] The process consists of three major steps: first, formation of liquid droplets from metal nanoparticles/clusters (*e.g.*, Au, Cu, Co, and Sn, *etc.*) as catalysts by thermal heating. Second, gas precursor decomposition followed by formation of a liquid alloy of the catalytic metal and growth materials. Finally, the growth material precipitates from the liquid alloy droplets upon supersaturation. The continuous supply of gas precursor results in the continuous growth of 1D nanomaterials. By now, a variety of 1D nanomaterials with acceptable diameter control and high crystalline quality have been prepared by this unique process.[13] However, it

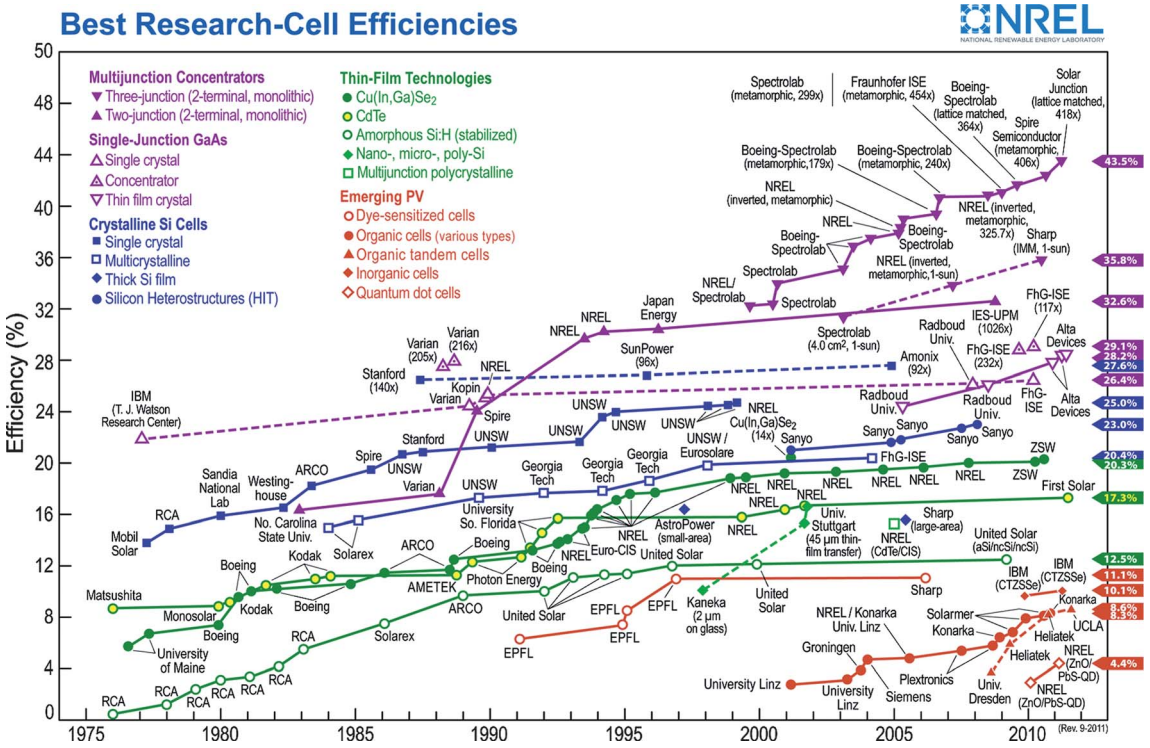

Fig. 3 Progression of record laboratory efficiencies for current solar cell technologies. (National Renewable Energy Laboratory (NREL), 2011).

is very challenging to control the spacing between nanowires using this approach.

Colloidal lithography or nanosphere lithography is a very simple, cost-effective, time-effective, and reproductive method to fabricate 1D nanowire and nanocone arrays with many materials on a large scale.[10,16] As shown in Fig. 4, the general fabrication process is as follows: First, monodisperse colloidal crystals are prepared on the substrate as masks through dip-coating, spin-coating, electrophoretic deposition, or Langmuir–Blodgett assembly, *etc.* The substrates are then etched by reactive ion etching (RIE). Depending on the conditions of RIE, either nanowires (Fig. 4c) or nanocones (Fig. 4d) can be obtained.

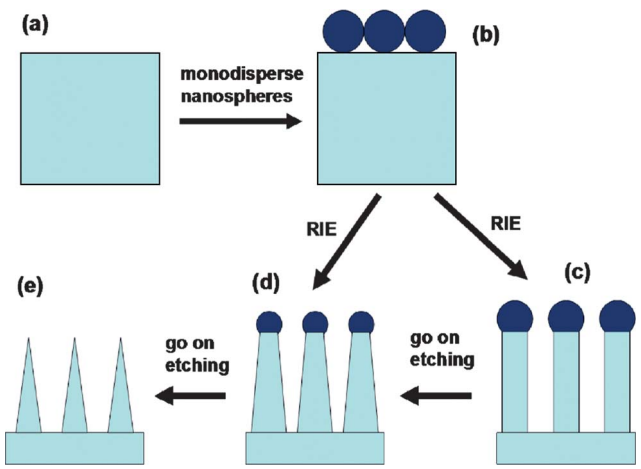

Fig. 4 Schematic procedure of fabricating nanowire and nanocone arrays by colloidal lithography.

Furthermore, the shape, diameter (*e.g.*, 60–600 nm) and spacing (50–400 nm) of these nanowire and nanocone arrays can also be rationally designed by controlling the RIE conditions such as etching time (Fig. 4e).[10]

Porous template-guided growth, which consists of filling the void spaces of a host porous medium with one or several desired materials, has been well developed to prepare a variety of nanowire and nanotube arrays.[17] Among the various templates, robust porous anodic aluminum oxide (AAO) templates have been demonstrated to be one of the most promising and most commonly used nanoporous materials. Until now, many different single metals (*e.g.*, Au, Ag, Ni, Co), alloys (*e.g.*, NiFe, CoFe), multilayers (*e.g.*, Co/Cu, NiFe/Cu), and conjugated polymers (*e.g.*, polypyrrole) have already been electrosynthesized in hard templates. For the growth of these materials, electrochemical deposition is the most commonly used approach. Meanwhile, metal catalytic CVD processes have also been performed to grow semiconductor nanomaterial arrays including Ge and CdS nanopillars, SnO_2 and ZnO nanowires, *etc.*[8,18]

Electrospinning is a simple and versatile technique for fabricating uniform fibers with diameters ranging from several micrometers down to a few nanometers.[19,20] In the process of conventional electrospinning, an electrostatic force generated by applied high voltage overcomes the surface tension of a droplet, and then a thin jet is ejected from the drop and rushes to the collector. The resultant fibers are usually deposited on the collector in the form of a nonwoven mat without orientation. In addition, parallel fibers and grid-patterned fibers with good orientation have also been electrospun through modified spinning approaches such as using a rotating cylinder collector, patterned collectors, a frame or gap collector, an auxiliary

electrical field or magnetic field, or centrifugal electrospinning.[19–21] A variety of materials such as polymer, metal, ceramic and glass have been electrospun into nanofibers, which have wide applications including optoelectronics, sensors, catalysis, textiles, filters, drug delivery, *etc.*[19,20]

3 Advantages of photovoltaics based on 1D nanostructure arrays

3.1 Improved anti-reflection and broadband absorption

As we know, the efficiency of a solar cell depends on the probability of an incident photon being absorbed, and the subsequent collection of the generated carriers, so solar cells surfaces with high absorbance and low reflectivity are often required. The current industrial standard of anti-reflection coating for thin-film solar cells is to use a quarter wavelength transparent layer with destructive interference. However, this technique only works for a narrow range of wavelengths.

Recently, reflection reduction and absorption enhancement have been widely observed in compound eyes of some nocturnal insects like moths, as well as 1D semiconductor nanostructure arrays.[8–11,16,23] For example, Zhu *et al.*[10] reported nanocone solar cells with an efficient broadband anti-reflection property and great processing advantages. As shown in Fig. 5a–b, between 400 and 650 nm, the absorption of nanocone arrays fabricated by the nanosphere lithography was maintained above 93%, which was much better than for either the nanowire array (75%) or thin film (64%). This is possibly due to the fact that the nanocones can scatter light along the in-plane dimension, and thus enhance the light traveling path for absorption. In addition, Fan *et al.*[22] presented a novel dual-diameter Ge nanopillar structure *via* template-guided synthesis, with a small diameter tip (*e.g.*, 60 nm) for minimal reflectance and a large diameter base (*e.g.*, 130 nm) for maximal effective absorption coefficient. As shown in Fig. 5c–d, these ordered dual-diameter pillar arrays with a thickness of only 2 μm showed an impressive absorbance of ~99% over a broad range of wavelengths of 300–900 nm.

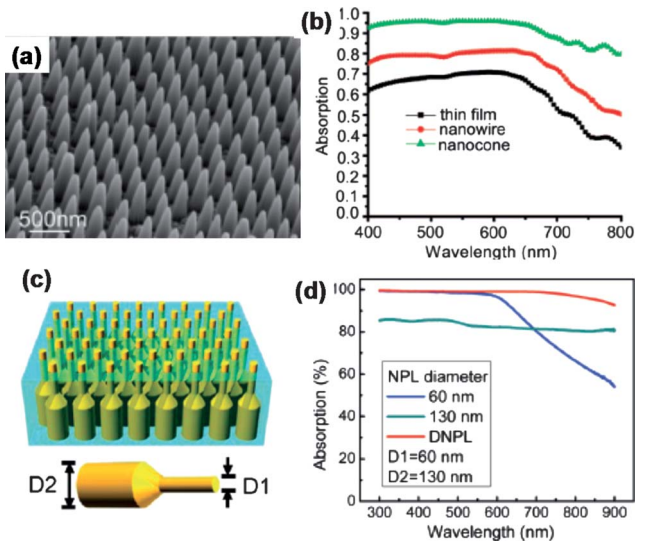

Fig. 5 (a) SEM image of amorphous Si:H nanocones prepared by nanosphere lithography. (b) Measured value of absorption on samples with a-Si:H thin film, nanowire arrays, and nanocone arrays as the top layer over a large range of wavelengths at normal incidence (reprinted from ref. 10 Copyright 2010, with permission from Elsevier Ltd.). (c) Schematic of a dual-diameter nanopillar array embedded in anodic aluminum oxide templates. (d) Experimental absorption spectra of a dual-diameter nanopillar array with $D_1 = 60$ nm and $D_2 = 130$ nm, and single-diameter nanopillar arrays with diameters of 60 and 130 nm (reprinted from ref. 22 Copyright 2010, with permission from the American Chemical Society).

Power conversion efficiency has also been enhanced for solar cells coated with these 1D nanostructure arrays. For instance, Forberich *et al.*[24] fabricated a type of organic solar cells by using a nano-replicated moth eye anti-reflection coating as an effective medium at the air-substrate interface, and the efficiency can be improved approximately 2.5–3% compared with solar cells without this structure. In another example, anti-reflective ZnO nanorod arrays were applied to InGaN-based multiple quantum well solar cells. It was found that the length of the nanorod arrays played an important role in the photovoltaic characteristics.[25] As a result, the 1.1 μm-long nanorod arrays enhance the conversion efficiency by ~36% due to the improved optical transmission. However, the 2.5 μm-long nanorod arrays lead to performances comparable to those of the bare surface despite their low reflection, which is attribute to the excessive absorption of the lengthened nanorods.

It is well known that the Fresnel reflection at an interface of two media is equal to $[(n_1 - n_2)/(n_1 + n_2)]^2$, where n_1 and n_2 are the refractive indices of the two media. The mechanism of biomimetic 1D nanostructure arrays which may suppress the reflection losses and increase transmission of incident light can be understood easily in terms of a gradient change in refractive index from the top of the structure to the bulk materials. Namely, the anti-reflection effect is usually due to the tapered shape of nanostructures with better effective refractive index matching with air.[10,16,26] However, through measuring maximum light trapping path length enhancement factors, Garnett and Yang[23] found that the light-trapping ability of Si nanowire solar cells was above the theoretical limit for a randomizing scheme, indicating that solar cells may show a photonic crystal enhancement effect. This result is consistent with the theoretical calculations. Due to the photonic crystal absorption enhancement effect in the presence of optical guided resonance modes,[27–31] vertical Si nanowire array solar cells with optimized photonic crystal architecture could lead to broad band solar-energy harvesting and offer conversion efficiency as high as 24% or more.[27] In addition, for plasmonic solar cells,[31] quantum dot/nanoparticle arrays have also been incorporated for absorption enhancement in the region close to bandgap edge owing to the large resonant scattering cross-section of these particles or plasmonics.

3.2 Enhanced carrier collection efficiency

In additional to enhancing optical absorption, arrayed 1D nanostructures can also significantly enhance the photo-carrier collection efficiency if the structure is properly designed.[6,8,9,32,33] The rationale can be schematically shown in Fig. 6a–b. It is known that photo-carrier collection and light absorption are in competition for planar structured solar cells. Efficient carrier collection requires thin materials to shorten the minority carrier travel

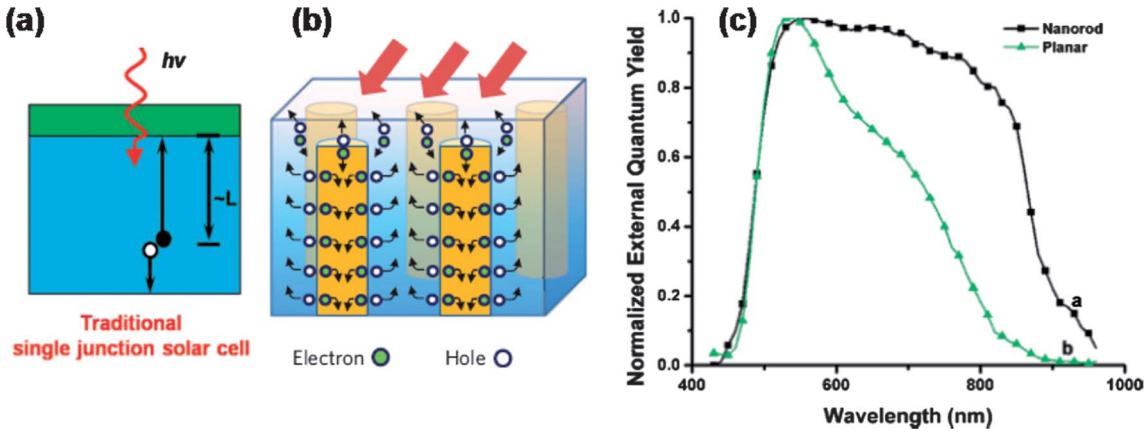

Fig. 6 Schematic of carrier collection in a planar thin film single junction solar cell (a) and a 3D nanowire/pillar solar cell (b) (reprinted from ref. 8 Copyright 2009, with permission from Nature Publishing Group). (c) Spectral response of typical photo-etched planar and nanorod array photoelectrochemical cells with the external quantum yield normalized to its highest value (reprinted from ref. 33 Copyright 2008, with permission from the American Chemical Society).

distance, and efficient light absorption requires thick materials for obvious reasons. This conflict may not be so severe in single crystalline Si as it has a minority carrier diffusion length in the hundreds of micrometers. However, the conflict is significant for poly-crystalline or even nanocrystalline materials which have relatively short carrier diffusion lengths. To greatly decrease the competition between carrier collection and light absorption, a 3D structure consisting of arrays of 1D nanomaterials for solar cells has been proposed. As shown in Fig. 6b, in such a structure, the p–n junction interface is parallel to light absorption direction, thus carrier collection occurs perpendicular to light absorption. An increase in the interface area of the p–n junction (compared with the planar structure) may significantly decrease the traveling distance for electron–hole pairs, and thus reduce the loss of electrons due to recombination. This mechanism works for both core/shell type p–n junction nanowire arrays and nanopillar/thin film hybrid devices. In fact, a comparison between nanorod arrays and planar Cd(Se,Te) photoelectrodes has been performed.[33] It was shown that the fill factors of the nanorod array photoelectrodes were superior to those of the planar junction devices. More importantly, the spectral response of the nanorod array photoelectrodes exhibited better quantum yields for collection of near-infrared photons relative to the collection of high-energy photons than the planar photoelectrodes, as shown in Fig. 6c.[33]

Furthermore, the performance benefit of orthogonalizing photon absorption and carrier collection was also demonstrated with the simulation of the CdS nanopillar/CdTe thin film hybrid solar cells.[8] In this work, the conversion efficiency of a device structure consisting of CdS nanopillar arrays embedded in a CdTe thin film were compared to that of a planar CdS/CdTe cell. The nanopillar structure showed improved conversion efficiency compared to its thin film counterpart, especially for small minority carrier diffusion lengths.[8] This result provides an important guideline for solar cell design using low cost and low grade materials.

3.3 Improved self-cleaning capability

Besides their high performance optical properties, the antireflective structure (ARS) arrays with high aspect ratios also exhibit self-cleaning capabilities due to the high fraction of air trapped in the trough area between nanopillars.[34–36] This function may provide one approach to solve the problem of dust particles accumulating on the solar cell surface and blocking the sunlight and thus reducing the power efficiency. For example, Min *et al.*[34] reported a templating technique using non-close-packed silica or close-packed polystyrene nanospheres as etching masks for fabricating broadband self-cleaning ARS surfaces with high aspect ratios (up to *ca.* 10) on both Si and glass substrates. Such ARS surfaces exhibit high performance antireflective properties. In addition, both surfaces are superhydrophobic and the measured apparent water contact angle was 172° for Si pillar arrays and 160° for the glass pillar arrays, which is significantly enhanced from 108° and 105° on fluorinated flat Si and glass substrates. Li *et al.*[35] have successfully prepared high aspect ratio Si hollow-tip arrays for high performance antireflective surfaces (Fig. 7a). The surfaces can suppress surface reflection from ultraviolet, visible light, to the mid-infrared region, with specular reflectance lower than 1% in the 250–1600 nm range. In addition, the tip arrays possess perfect water-repellent properties (with a measured apparent water contact angle of 165° and a small sliding angle of 2°) due to their high aspect ratio, as shown in Fig. 7b.

In addition to superhydrophobic ARS surfaces, Li *et al.*[36] also prepared large area superhydrophilic ARS arrays on planar

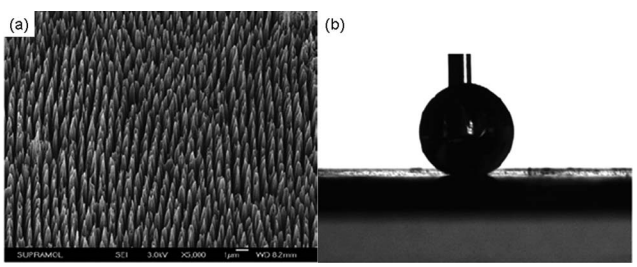

Fig. 7 (a) SEM image of the hollow-tip arrays, and (b) an optical image of the water droplet profile (5 mL) on the silicon hollow-tip array surface (reprinted from ref. 35 Copyright 2009, with permission from The Royal Society of Chemistry).

fused silica substrates for high performance ARS and antifogging surfaces. The ARS surfaces can dramatically increase the hydrophilicity of the silica substrate because of the increased surface roughness of the hydrophilic silica substrate, and the water droplet completely spreads over the surface within 0.66 s. Such superhydrophilic surfaces can dramatically suppress the fogging behaviour because the condensed water droplets will spread flat instantaneously to form a thin sheet-like water film. The ARS surfaces with water-repellent or antifogging properties enable the application of the devices in humid environments.

4 Three-dimensional nanostructured solar cells

4.1 Solar cells based on Si, Ge or GaAs nanowire/pillar arrays

4.1.1 Si nanowire/pillar-based solar cells. Solar cells based on Si nanowires have drawn more and more interest in recent years for their strongly enhanced light trapping, high carrier collection efficiency and potential low cost, and a large number of promising works have been done on this series of materials. For instance, Tian *et al.*[7] have fabricated individual radial p–i–n coaxial Si nanowire structures consisting of a p-type Si nanowire core capped with i- and n-type Si shells. The open circuit voltages V_{oc}, short circuit current I_{sc} and fill factor FF are measured as 0.26 V, 0.503 nA and 0.55, respectively. The p–i–n Si nanowire elements yield a maximum power output of up to 200 pW per nanowire device and an apparent energy conversion efficiency of up to 3.4% after exclusion of the metal covered area. After that, large area arrays of Si nanowires with radial p–n junctions have been reported. For example, Garnett *et al.*[23] have demonstrated a simple and scalable method to fabricate large-area ordered Si nanowire radial p–n junction photovoltaics (Fig. 8a). The method requires dip coating a Si substrate to self-assemble SiO_2 spheres, followed by deep reactive-ion etching (DRIE) to form ordered nanowires and diffusion to form the p–n junction. A maximum light trapping path length enhancement factor, depending on the nanowire geometry, over the entire AM 1.5G spectrum between 1.7 and 73 were measured. This agrees well with enhancement factors between 2 and 62 extracted from optical transmission measurements. Their efficiencies are above 5%, with short circuit photocurrents higher than those of planar control samples. Bao *et al.*[37] have performed further research on such nanowires, and their investigation demonstrates that ordered nanowire arrays with random-diameters show significantly broadened and enhanced absorption, while random-length nanowire arrays show both significantly reduced reflection and enhanced absorption. The absorption enhancement can be attributed to the enhanced interwire multiple scattering and/or inner-wire resonance in the random array structure. In addition, Baek *et al.*[38] have observed the relationship between the wire length and cell performance. That is, the beneficial effects of the Si solar cells are derived from the better light trapping property with increasing wire length. Moreover, high-efficiency (up to 10.8%) solar cells have been achieved using a new large-area ordered Si nano-conical-frustum (NCF) array (Fig. 8b) by self-powered parallel electron lithography (SPEL).[39] The NCF array structure exhibits an impressive absorbance of ~99% (upper bound) over the wavelengths 400–1100 nm with a thickness of only 5 μm. The solar cells with ordered Si NCF arrays (800 nm lattice constant) had a short circuit current density (J_{sc}) of 26.4 mA/cm^2, V_{oc} of 0.59 V, FF of 0.69, and an efficiency of 10.8%. Although these NCF structure arrays have high light absorption efficiency, the solar cell efficiency is still less than half of that for bulk crystalline Si solar cells and the V_{oc} and FF are lower too. This is probably due to the high surface recombination losses, which are introduced by the highly enhanced surface area from the nanostructures, although a thin passivation oxide layer was used.

In addition, Kuang *et al.*[40] have employed an ultrathin hydrogenated amorphous Si (a-Si:H) n-i-p junction deposited on ZnO nanorod arrays, and the cross-sectional structure schematic is shown in Fig. 8c. In this case, an efficiency of 3.6% and a short-circuit current density of 8.3 mA cm^{-2} were obtained, significantly higher than values achieved from planar or even textured counterparts with a-Si:H absorber layers thickness of 75 nm.

4.1.2 Solar cells based on Ge or GaAs nanowire/pillar arrays. Ge is an excellent light absorption material due to its small band-gap. For example, self-organized anodic Al_2O_3 membranes were used as templates for the vapour–liquid–solid growth of ordered, single-crystalline Ge nanopillar arrays on Al foil with controlled shape and dimensions. A dual-diameter Ge nanopillar structure is demonstrated by Fan *et al.*,[22] as shown in Fig. 9a–b. It enables fine control over geometry and shape of nanopillar arrays, without the use of complex epitaxial and/or lithographic processes. Here, a small diameter tip for minimal reflectance and a large diameter base for maximal effective absorption coefficient

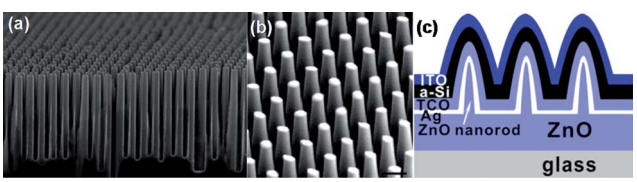

Fig. 8 (a) Tilted cross-sectional SEM image of the Si nanowire solar cell (reprinted from ref. 23 Copyright 2010, with permission from the American Chemical Society). (b) The side view (45°) SEM image of the ordered Si NCF arrays, with scale bar 800 nm (reprinted from ref. 39 Copyright 2010, with permission from the American Chemical Society). (c) Cross-sectional schematic of ZnO-nanorod/a-Si:H solar cells (reprinted from ref. 40 Copyright 2011, with permission from the American Institute of Physics).

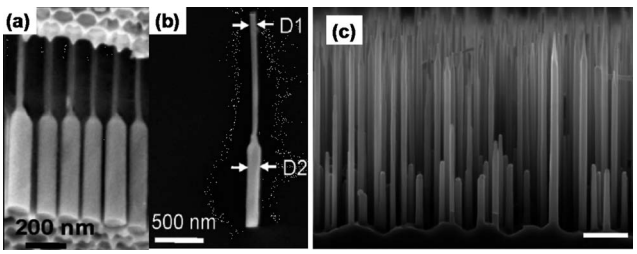

Fig. 9 (a) Cross-sectional SEM image of Ge dual-diameter nanopillars after the growth in anodic aluminum oxide (AAO) membranes. (b) SEM of a single Ge dual-diameter nanopillar (reprinted from ref. 22 Copyright 2010, with permission from the American Chemical Society). (c) SEM image of the GaAs core/shell nanowires (reprinted from ref. 43 Copyright 2009, with permission from the American Chemical Society).

are required. The Ge NPL arrays exhibit an impressive absorbance of ~99% for $\lambda = 300$–900 nm. Peköz *et al.*[41] have analyzed the properties of the designed Ge/Si and Si/Ge core/shell and Si–Ge layered nanowires using a mathematical method. Both core/shell and layered nanowires have a strong charge-carrier separation, with electron states mainly on Si atoms and hole states on Ge atoms. This charge separation also potentially makes it easier to design and deposit effective contacts, either by the selective etching technique for the Si/Ge (Ge/Si) core/shell nanowires, or by direct connection in the case of the triangularly shaped, layered Si/Ge nanowires. It is believed that they all show promising features for use in photovoltaic applications by overcoming some of the existing problems.[41]

Si (or Ge) has many advantages for conventional planar solar cells, but due to its low optical absorption coefficient and small band gap, it may not be the only ideal material for nanowire solar cells. In comparison, GaAs has a larger optical absorption coefficient and nearly ideal band gap ($E_g = 1.45$ eV), although it still suffers from high surface recombination velocities. With efficiency $\eta = 4.5\%$ and fill factor FF = 0.65 under AM 1.5G illumination, Colombo *et al.*[42] have reported radial p–i–n diode nanowire solar cell devices based on GaAs. At the same time, LaPierre *et al.*[43,44] fabricated GaAs radial p–n nanowires with the single nanowire devices (Fig. 9c), and they exhibit $\eta = 0.8\%$ and FF = 0.26. Further research on GaAs nanowire solar cells has been continued by the same team. Also a numerical simulation of current–voltage characteristics of III–V nanowire core/shell p–n junction diodes under illuminated conditions is presented with an emphasis on optimizing the nanowire design for photoconversion efficiency. The calculation shows that the detailed balance efficiency of ~30% can be nearly achieved in a radial p–n junction with top contact geometry and minimal tip height, assuming that ohmic contacts and effective surface passivation can be implemented.[44]

4.2 CdS/CdTe nanopillar based solar cells

Since the 1.45 eV band gap of CdTe is nearly optimal for absorbing sunlight and CdS/CdTe compound semiconductors have much lower surface recombination velocities as compared to that of Si, this material system has been typically fabricated as polycrystalline films for solar cell applications. Several studies have focused on improving the efficiency of CdTe/CdS-based solar cells. For example, the Ready group has used vertically aligned periodic arrays of carbon nanotubes (CNTs) to create topographically enhanced light-trapping CdS/CdTe solar cells.[45] As shown in Fig. 10a, these 3D cells were composed of regularly spaced towers consisting of vertically aligned CNTs grown by CVD, which formed the back contact of the cell and served as a scaffold to support the photoactive hetero-junction. Then CdTe and CdS were deposited as the p/n-type materials by molecular beam epitaxy (Fig. 10b), and a conformal coating of indium tin oxide (ITO) was deposited as the transparent collection electrode. Due to multiple scattering process, the 3D cells exhibited a high current density (44.4 mA cm^{-2}) and increased power production at off-normal angles. Efficiency was shown to double from 3.5% at an orthogonal "high noon" azimuthal angle to 7% at a 45° solar incidence (Fig. 10c).[45] Simulated modeling also showed that by optimization of geometrical parameters, such a 3D cell could obtain up to a 300% increase in power production over traditional cells.[46]

In particular, Fan *et al.*[8] have demonstrated a low cost nanopillar solar cell consisting of an array of CdS nanopillars partially embedded in a CdTe thin film (Fig. 11a). The nanopillar solar cells are fabricated as follows: first, n-type CdS nanopillars were grown by CVD in a porous anodic alumina membrane (AAM) with Au seeds as catalysts, which were electrochemically deposited at the bottom of the pores. Then the processed AAM was partially and controllably etched in a sodium hydroxide solution to expose the upper portion of the pillars to form the 3D structures. After that, a p-type CdTe thin film was deposited by CVD to serve as the photo-absorption layer. The top Cu/Au electrode was finally deposited by the thermal evaporation. In such a configuration, the backside electrical contact to the n-type CdS nanopillars was simply the Al support substrate. The cell performance was characterized under different illumination condition from 17 to 100 mW cm^{-2}. Under AM 1.5G illumination, the cell produced a short circuit current density of ~21 mA cm^{-2}, an open circuit voltage of ~0.62 V and a fill factor of ~43%, yielding an efficiency of ~6% (Fig. 11b). Besides using rigid substrates, nanopillar solar cell fabrication was also performed on plastics such as polydimethylsiloxane (PDMS) for flexible and high performance photovoltaics (Fig. 11c). It was found that the flexible nanopillar solar cell module exhibited negligible change in the cell performance, such as the energy conversion efficiency, under different bending conditions. In addition, further studies indicated that the conversion efficiency of CdS/CdTe solar nanopillar cells could be improved to over 20% through materials and device optimization.[47]

4.3 DSSCs based on TiO_2 and ZnO nanowire/tube arrays

4.3.1 ZnO and TiO_2 nanowires/rods. As shown in Fig. 12a, a ZnO nanowire dye-sensitized solar cell (DSSC) reported by Law *et al.*[6] in 2005 catalyzed research on 1D nanomaterial-based photovoltaics. The report demonstrated that 1D nanostructures might provide direct pathways for electron transport, longer diffusion length and higher charge collection efficiencies. In their work, vertical arrays of ZnO nanowires with diameters of ~130 nm were grown on F:SnO_2 (FTO) glass substrates by immersing seeded substrates in aqueous solutions. Photovoltaic measurements showed device characteristics of a short circuit current of 5.3–5.85 mA cm^{-2}, an open circuit voltage of 0.61–0.71 V, and a conversion efficiency of 1.2–1.5%. It was found that the ZnO nanowires had high electron diffusivity, 0.05–0.5 cm^2 s^{-1}, several hundred times larger than that typically used in ZnO nanoparticle films. The charge collection efficiency of ZnO nanowire photoanodes, ~55–75%, was also much higher than that of electrodes made of ZnO nanoparticles.[6] In addition, flexible DSSCs based on vertical ZnO nanowire arrays on ITO-coated poly(ethylene terephthalate) substrates were demonstrated (Fig. 12b).[48] Besides ZnO nanowire arrays,[6,48–51] TiO_2 nanowire DSSCs were also recently reported.[52–54] For example, an overall conversion efficiency of 5–6% was obtained,[53,54] which is obviously much higher than that of ZnO nanowire DSSC (1.2–1.5%). The improvement is attributed to a higher electron injection efficiency from excited dye molecules into the

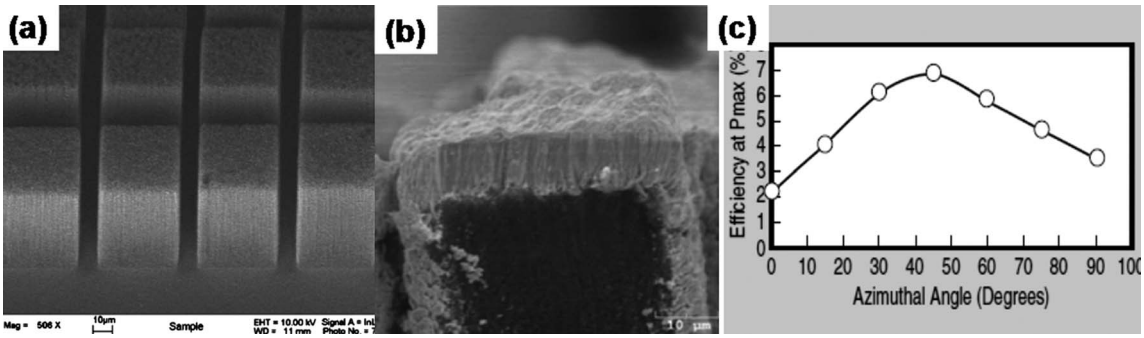

Fig. 10 (a) SEM image of as grown array of vertically aligned CNT towers. (b) Cutaway view of individual CNT tower (black) coated with CdTe (gray) and CdS. (c) The corresponding increase in efficiency for CNT-cell with respect to azimuthal angle (reprinted from ref. 45 Copyright 2007, with permission from Springer-Verlag).

TiO_2 conduction band and/or a higher dye regeneration efficiency than that in ZnO.[55]

Here it should be noted that in order to improve device performance, an interesting new approach to fabricate high-efficiency 3D DSSCs by integrating planar waveguides and aligned ZnO nanowire arrays was recently presented.[56] The ZnO nanowires were grown normally on both surfaces of the quartz slide, which served as a planar waveguide for light propagation. As shown in Fig. 12c, the 3D DSSC is constructed by alternatively sandwiching the quartz slides and the planar Pt electrodes. The 3D cell can effectively increase the light absorbing surface area due to internal multiple reflections without increasing electron path length to the collecting electrode. On average an enhancement of energy conversion efficiency by a factor of 5.8 has been achieved when light propagating inside the slide is compared to the case of light illumination normal to the surface of the slide from outside. Moreover, full sun efficiencies have been achieved up to 2.4% for ZnO nanowires.[56]

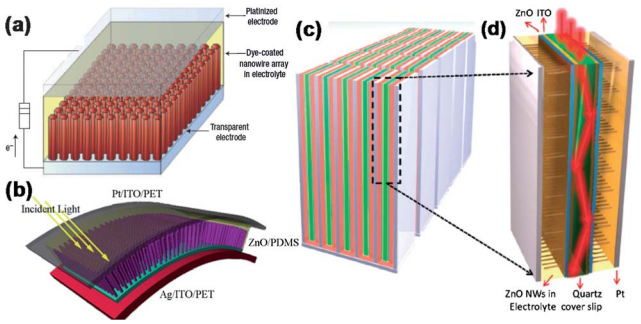

Fig. 12 (a) Schematic diagram of a ZnO nanowire array DSSC (reprinted from ref. 6 Copyright 2005, with permission from Nature Publishing Group). (b) Schematic view of a flexible ZnO nanowire array DSSC (reprinted from ref. 48 Copyright 2011, with permission from the Springer Group). (c) Schematic architecture of planar waveguide-nanowire integrated 3D DSSC. (d) Detailed structure of a unit waveguide-nanowire 3D DSSC (reprinted from ref. 56 Copyright 2010, with permission from the American Chemical Society).

4.3.2 TiO_2 and ZnO nanotubes. Since hollow structured nanotubes may provide a larger surface area than that of nanowires and nanorods, DSSCs based on TiO_2[50,57–61] and ZnO nanotubes[62–64] have drawn attention in the past years. Macák *et al.* reported for the first time in 2005 that TiO_2 nanotubes prepared by a simple anodic oxidation of titanium foil might have a DSSC application.[57] For back-side illumination of the DSSCs (the light comes from the counter electrode), a maximum of 4.24% efficiency has been obtained for a photoelectrode film that is comprised of ~6 μm long TiO_2 nanotubes. For front-side illumination (the light comes from the photoelectrode) with a 35 μm-thick TiO_2 nanotube photoelectrode film, a conversion efficiency as high as 7% has been reported.[60] In addition, $TiCl_4$ treatment of the TiO_2 nanotubes can also improve the conversion efficiency.[57,61] However, for ZnO nanotube DSSCs,[62–64] the

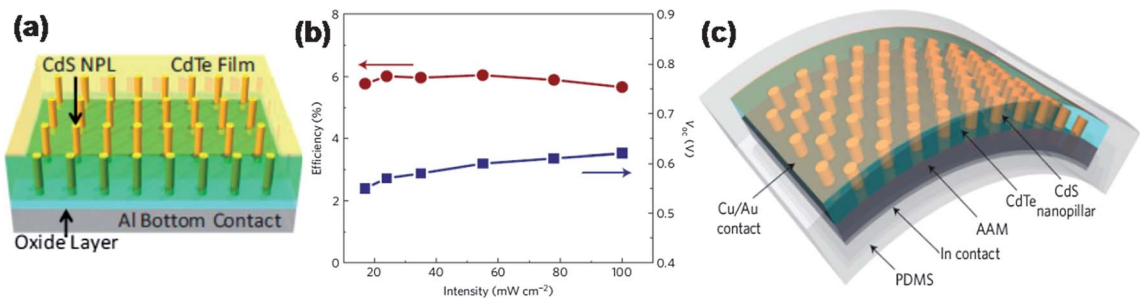

Fig. 11 (a) Schematic of a solar nanopillar cell consisting of an array of CdS nanopillars partially embedded in a CdTe thin film. (b) The open-circuit voltage slightly increases with the intensity and the solar energy conversion efficiency is nearly independent of the illumination intensity for 17–100 mW cm^{-2} (reprinted from ref. 8 Copyright 2009, with permission from Nature Publishing Group). (c) Schematic diagram of a bendable solar nanopillar cell module embedded in PDMS (reprinted from ref. 47 Copyright 2010, with permission from the American Institute of Physics).

conversion efficiencies so far achieved were generally low (~1.2–1.6%). A possible reason is that the length and surface area of the ZnO nanotubes are limited by the fabrication methods such as etching ZnO nanorods[62] or template growth.[64]

4.3.3 Hybrid nanowires/nanoparticles or core/shell nanostructures. The power conversion efficiency of the nanowire/tube DSSC can be further improved by increasing the internal surface area of the photoelectrode *via* filling the interstices of nanowire/tube array films with nanoparticles,[65–69] or reducing the interfacial recombination rate *via* applying surface coatings on the nanowire array films.[70–72] For DSSCs based on hybrid nanostructures of nanowires/tubes (serving as a direct pathway for fast electron transport) mixed with nanoparticles (offering a high specific surface area for sufficient dye adsorption), most of the studies were carried out on array films of ZnO or TiO_2 nanowires, or TiO_2 nanotubes filled with ZnO or TiO_2 nanoparticles. For example, a significant increase in the conversion efficiency from 0.5–0.8% to 2.2–3.2% has been achieved in a DSSC based on ZnO nanowire arrays filled with ZnO nanoparticles.[65] The efficiency of a ZnO nanowire– nanoparticle hybrid DSSC could be further improved to ~4.2% (Fig. 13).[68] Alivov *et al.*[69] also demonstrated that a photoelectrode made of TiO_2 nanotube array film filled with ~10 nm TiO_2 nanoparticles could increase the cell efficiency from 3.81% to 5.94%.

Since a surface barrier can reduce the charge recombination, core/shell structure with a coating layer on nanowire array film is also effective in enhancing photovoltaic performance. For instance, Law *et al.*[70] reported that ZnO nanowires coated by 10–25 nm-thick TiO_2 could increase the open circuit voltage of the DSSC and lead to an enhancement in the conversion efficiency from 0.85% to 1.7–2.1%. An improved efficiency from 2.1% for bare SnO_2 nanowires to 4.1% for TiO_2-coated SnO_2 nanowire photoelectrode was also achieved.[71] In another work, the cell performance of the ZnO nanowire-based DSSCs was greatly improved by the deposition of a thin ZnS shell onto the ZnO nanowires. The conversion efficiency was increased from 0.11% to 2.72%, which was resulted from the reduced visible absorption of the anode semiconductor and the reduced defect sites on the surface (which suppresses recombination of injected electrons).[72] Furthermore, electrochemical deposition of CdSe onto TiO_2 nanorod arrays can also extend absorption into the visible light region and improve the photovoltaic performance.[73a] The ZnO/$Zn_xCd_{1-x}Se$ ($0 \leq x \leq 1$) core/shell nanocable arrays were demonstrated to be promising photoelectrodes for photoelectronchemical solar cells, giving a maximum conversion efficiency up to 4.74%.[73b]

4.3.4 3D hierarchical or aggregate nanostructures. Recently, three-dimensional (3D) hierarchical or aggregate nanostructure photoelectrodes in DSSC applications have drawn much attention due to the relatively large surface area, effective light harvesting, charge transport and charge collection. As shown in Fig. 14, a variety of 3D nanostructures such as ZnO nanotetrapods,[74,75] branched ZnO nanowires,[76] ZnO or TiO_2 nanoforests,[77,78] dendritic ZnO nanowires,[79] ZnO nanoflowers,[80] ZnO aggregates,[81] TiO_2 nanotubes on titanium mesh,[82] nanoporous TiO_2 spheres,[83] and hollow TiO_2 hemispheres[84] have been reported. It was found that these 3D nanostructure photoelectrodes can indeed improve photovoltaic performance. For example, an efficiency of 3.27% was reported for a photoanode film consisting of ZnO nanotetrapods,[74] which was much higher than those obtained for ZnO nanowire/rod/tube arrays (~1.2–2.0%). Particularly, DSSCs based on ZnO or TiO_2 nanoparticle aggregates exhibited very high conversion efficiency of 5.4%[81] and 10.5%,[83] respectively, possibly due to very the high surface area, strong light scattering and short diffusion distance.[81,83] Furthermore, recent investigations demonstrated that hybrid structures of ZnO nanotetrapods/SnO_2 nanoparticles,[75,85] hierarchical ZnO[86] or TiO_2 nanodendrites/nanoparticles[87] may be promising photoelectrodes for high-efficiency DSSCs.

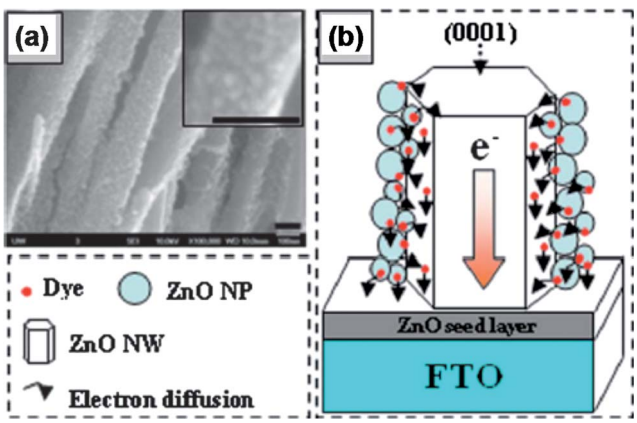

Fig. 13 (a) SEM image of ZnO nanoparticles on the surface of ZnO nanowires in the hybrid ZnO nanowire–nanoparticle photoanode, scale bars 100 nm. (b) Schematic representation of the possible electron path way (along the nanowire) in the hybrid nanowire–nanoparticle photoanode (reprinted from ref. 68 Copyright 2010, with permission from the American Institute of Physics).

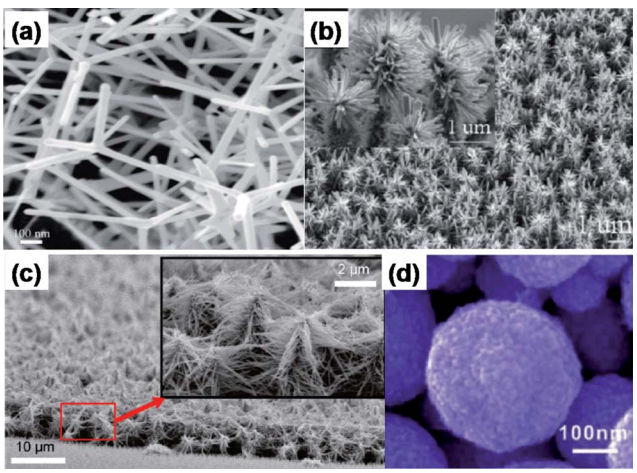

Fig. 14 SEM images of (a) ZnO nanotetrapods (reprinted from ref. 74 Copyright 2009, with permission from Elsevier Ltd.). (b) Branched ZnO nanowires (reprinted from ref. 76 Copyright 2008, with permission from the American Chemical Society), (c) ZnO nanotrees and nanoforest (reprinted from ref. 78 Copyright 2011, with permission from the American Chemical Society), and (d) ZnO aggregates consisting of nanocrystallites for DSSC applications (reprinted from ref. 81 Copyright 2008, with permission from WILEY-VCH Verlag GmbH & Co. KGaA).

5 Solar cells based on electrospun nanofibers

5.1 Electrospun nanofibers as DSSC photoelectrodes

5.1.1 TiO_2 and ZnO nanofibers. Electrospinning is a simple, low cost and versatile production method to prepare various continuous 1D fibers on a large scale, including polymers, ceramics and composites.[19–21] Since electrospun nanofibers can offer high specific surface areas (10^2–10^3 m^2 g^{-1}) and bigger pore sizes, much effort has been invested in the past a few years toward their application in dye-sensitized solar cells such as photoanodes and electrolytes.[12,88,89] Furthermore, compared with nanoparticle film-based DSSCs whose high efficiencies are often limited due to their disordered geometrical structures and interfacial interference in electron transport, nanofiber-based photoelectrods can offer direct pathways for electron transport, give larger electron diffusion length, and therefore provide enhanced energy conversion efficiencies in DSSCs. The highest efficiency for electrospun DSSCs reported to date has reached 10.3%.[90] Several electrospun materials such as TiO_2 and ZnO nanofibers have been utilized in DSSCs. For example, Song *et al.*[91] reported electrospun TiO_2 single-crystalline nanorods which were composed of nanofibrils with an islands-in-a-sea morphology (Fig. 15a). The nanorod electrode (Fig. 15b) provided efficient photocurrent generation in a quasi-solid-state DSSC, which showed overall conversion efficiency of 6.2% under AM 1.5G illumination.[91] In addition, multiple networks of ZnO nanofibers were prepared using electrospinning followed by hot pressing and calcination steps. They were composed of a twisted structure of 200–500 nm diameter cores with ~30 nm single grains (Fig. 15c). The DSSCs based on these ZnO nanofiber mats exhibited a conversion efficiency of 1.34% under 100 mW cm^{-2} illumination.[92]

5.1.2 Cross-aligned and vertically aligned nanofibers. In addition to randomly oriented nanofibers, TiO_2 and ZnO nanofibers have been electrospun in an aligned or crossed architecture in order to enhance the exciton dissociation area and the charge conduction on the hybrid solar cell. For example, as shown in Fig. 16a, Shim *et al.*[93] demonstrated hybrid solar cells fashioned of planar-aligned TiO_2 nanofiber architectures such as uniaxially aligned nanofibers (Fig. 16b) and multiple layers of cross-aligned nanofiber arrays (Fig. 16c) with poly[2-methoxy-5-(2′-ethyl-hexyloxy)-1,4-phenylenevinylene] (MEH-PPV). It was found that the active layer composed of the aligned TiO_2 nanofiber array and MEH-PPV polymer showed better photoluminescence quenching (which should be associated with the charge separation efficiency) under similar light absorption as compared to disordered TiO_2 nanofibers. Therefore, as shown in Fig. 16e, the photoinduced current (1.28 mA cm^{-2}) and power conversion efficiency of the cells could be significantly improved by at least 50% under 1 sun conditions depending on the degree of aligning fibers.[93] In addition, Yan *et al.*[94,95] also reported hybrid solar cells based on ordered electrospun TiO_2 and ZnO nanofiber arrays with conjugated poly(3-hexylthiophene) (P3HT), and they found that the organic–inorganic hybrid cells with 3 cross-aligned layers showed enhanced photovoltaic performance. Moreover, DSSCs with vertical nanofibers of electrospun TiO_2 as a photoelectrode were recently reported.[96] The aligned nanofibrous TiO_2 ribbons were firstly produced by electrospinning, and then erected to vertical nanofibers (Fig. 16d) after post-treatment of rolling up, stacking and cutting. The conversion efficiency, short circuit current, and open circuit voltage of the resultant DSSC were measured as 2.87% and 5.71 mA cm^{-2}, 0.782 V respectively (Fig. 16f).

5.1.3 Nanofiber-nanoparticle composites. In an effort to maintain both a high surface area and efficient charge transport, a combination of electrospun nanorods/nanofibers and nanoparticles has been proposed. For example, Fujihara *et al.*[97] reported a solar cell with two TiO_2 layers: a ground electrospun TiO_2 nanoparticle layer on a glass plate and then a TiO_2 nanorod layer. It was found that the devices with a combination of electrospun nanorods and nanoparticles showed improved conversion efficiencies over the entirely nanorod devices. Chuangchote *et al.*[90] also suggested that nanofiber-modified nanoparticles are

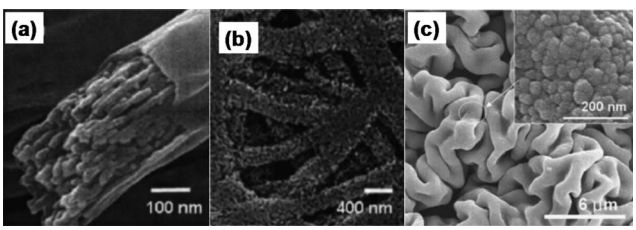

Fig. 15 (a) SEM image of a TiO_2 fiber showing an islands-in-a-sea morphology with nanofibrils. (b) SEM image of TiO_2 nanorod electrode (reprinted from ref. 91 Copyright 2005, with permission from the American Institute of Physics). (c) SEM image of ZnO nanofiber mats hot pressed at 120 °C and calcined at 450 °C. The inset exhibits the networks of twisted nanofibers composed of individual grains of ~30 nm (reprinted from ref. 92 Copyright 2007, with permission from the American Institute of Physics).

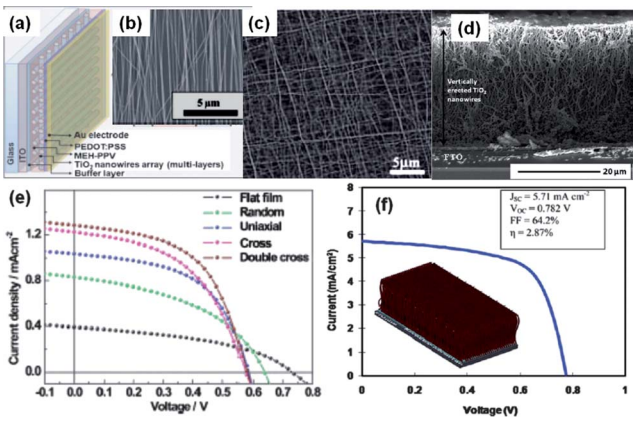

Fig. 16 (a) Schematic illustration of a hybrid solar cell introduced with aligned TiO_2 or ZnO nanofibers *via* electrospinning. SEM images of uniaxially aligned TiO_2 nanofibers (b), cross-aligned TiO_2 nanofibers (c) and vertically erected TiO_2 nanowires (d). Current–voltage (*J*–*V*) characteristics of (e) MEH-PPV:TiO_2 hybrid solar cells depending on different configurations of aligned TiO_2 nanofibers, and (f) a DSSC based on vertical TiO_2 nanowires array electrode. (reprinted from ref. 93 Copyright 2008, with permission from the American Institute of Physics, and ref. 96 Copyright 2011, with permission from the Royal Society of Chemistry).

very promising materials for the electrode structure of DSSCs. In their work, TiO_2 nanofibers were fabricated directly onto thick nanoparticle electrodes by using electrospinning and sol–gel techniques. The DSSCs comprised of a nanoparticle/nanofiber electrode showed an incident photon-to-current conversion efficiency (IPCE) of 85% at 540 nm with conversion efficiencies of 8.14% and 10.3% for areas of 0.25 and 0.052 cm^2, respectively. Here it is noted that the conversion efficiency of 10.3% is the highest reported efficiency for electrospun DSSCs. More recently, a composite photoanode made of electrospun TiO_2 nanofibers and conventional TiO_2 nanoparticles (15% nanofibers and 85% nanoparticles by weight) was reported.[98] Fig. 17 shows schematic illustration of the nanofiber/nanoparticle solar cell, which noticeably improved the light harvesting through the enhancement of Mie scattering without substantially sacrificing the dye uptake in DSSCs. With the same fabrication conditions and film thickness, the DSSCs demonstrated 44% higher device efficiency than those made from TiO_2 nanoparticles alone. In addition, the photovoltaic performance of electrospun DSSCs can be improved by creating hollow microtubes within the TiO_2 layer (these tubes act as light-scattering centers and thus increase the optical path length)[99] or improving the adhesion of electrospun fibers to the substrate.[92]

5.2 Quasi-solid-state DSSCs with electrospun membrane electrolytes

Besides the photoelectrodes, electrospun polymer nanofiber films can be also used as solid or semi-solid electrolytes instead of the traditional liquid electrolytes within DSSCs in order to improve durability and stability. This is because the electrospun polymer fiber films have lots of inter-connected pores that help to encapsulate electrolyte solution. For instance, Priya *et al.*[100] reported a quasi-solid-state solar cell with an electrospun poly(vinylidenefluoride-*co*-hexafuoropropylene) (PVDF-HFP) membrane electrolyte. As shown in Fig. 18a, the cell was fabricated by sandwiching a slice of the PVDF-HFP membrane electrolyte between a dye-sensitized TiO_2 electrode and a Pt counter electrode. The cell showed an open-circuit voltage of 0.76 V, a fill factor of 0.62, and a short-circuit current density of 15.57 mA cm^{-2} at an incident light intensity of 100 mW cm^{-2}. Although this cell showed a slightly lower solar energy-to-electricity conversion efficiency (7.3%) than the conventional liquid electrolyte solar cells (7.8%), the cell exhibited better long-term durability by preventing electrolyte leakage. Fig. 18b shows the conversion efficiency variation over time for a liquid electrolyte and an electrospun PVDF-HFP membrane electrolyte, respectively. It is evident that the quasi-solid-state solar cells remain at 96% of its initial value after 13 days. In addition, Kim *et al.*[101] also found that the photovoltaic performance of DSSC devices was improved by using electrospun PVDF-HFP nanofiber membranes.

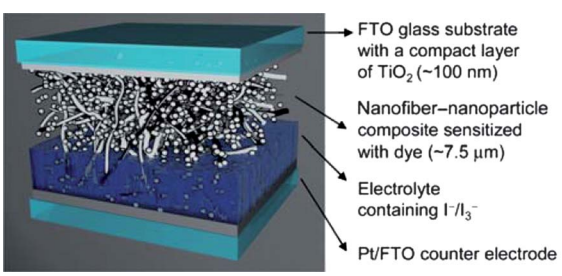

Fig. 17 Schematic illustration of a nanofiber-nanoparticle composite solar cell (reprinted from ref. 98 Copyright 2010, with permission from the Royal Society of Chemistry).

6 Summary and outlook

In this paper, we briefly reviewed a variety of solar cells based on 1D nanomaterials. 1D nanomaterials have mesoscopic dimensions which result in intriguing physical properties, including large surface area, quantum confinement effects, enhanced photon absorption and excellent mechanical flexibility. Therefore, nanostructured solar cells usually show improved reflection reduction, and absorption enhancement over a broadband spectrum and a wide range of incidence angles, and may even show enhanced carrier collection efficiency and self-cleaning capacity. These aspects suggest that 1D nanomaterials can be potential candidates for next generation cost-effective photovoltaics by providing a way to reduce both the quantity and quality of the required semiconductor.

Despite the incredible light trapping property, solar cells based on 1D nanostructure arrays still do not exceed the overall efficiency of the corresponding planar cells in many cases, for example, Si layers above 8 μm in thickness.[23] The possible reason is enhanced recombination of charge carriers through surface states, which reduces the carrier diffusion lengths in 1D nanostructures by a few orders of magnitude.[102] Since surface passivation is important for high-performance planar solar cells and may be even more critical for nanostructured photovoltaics, proper surface treatments and improved array geometries will be significant for achieving high efficiency solar cells based on 1D nanostructure arrays.[10,23,103] For instance, Dan *et al.*[103] showed that a thin layer of amorphous Si coated on a single-crystalline Si nanowire can reduce the surface recombination by nearly 2 orders of magnitude due to the enhanced carrier lifetime by surface passivation. This demonstrates an important approach for the realization of high-performance nanosized optoelectronic devices.

It should be noted that besides the widely reported arrays of 1D nanowires, nanopillars, nanorods, nanotubes, and nanofibers, recent studies have demonstrated that solar cells based on nanohole arrays (Fig. 19a–b),[104–107] zigzag structure arrays,[108] branched nanowire arrays or nanoforests,[77,78] nanocrystallite aggregates,[81,83] nanograting arrays,[109] nanospike arrays,[110] and nanocomposites of 0D and 1D materials,[68,69,75,85–87,98] *etc.* also show superior light trapping capability and thus, higher power conversion efficiency. For example, Si nanohole texturing can give a high short-circuit current of ~37.3 mA cm^{-2}, as compared to Si nanopillar texturing (~31.9 mA cm^{-2}) and a Si thin film reference (~10.5 mA cm^{-2}). Accordingly, as shown in Fig. 19c, the power conversion efficiency of Si nanohole textured thin film photovoltaic device can reach 20.5%, as compared to the 17.6% achieved by a Si nanopillar array textured photovoltaic device.[106] These results open up new designs and exciting opportunities for a variety of photovoltaics to further improve the device performance.

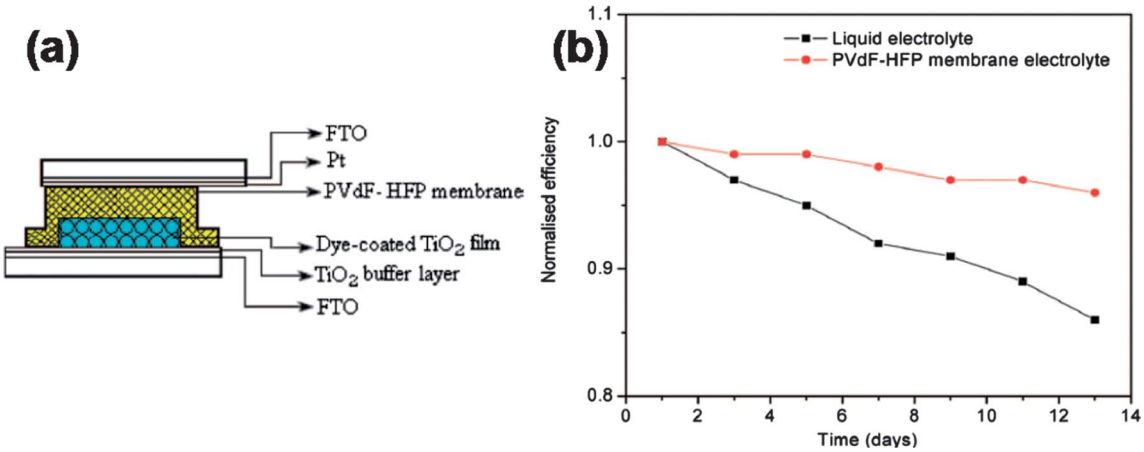

Fig. 18 (a) Schematic diagram of a quasi-solid-state DSSC with electrospun PVDF-HFP membrane electrolyte. (b) Normalized light-to-electricity conversion efficiency variation of the DSSCs with liquid electrolyte and electrospun PVDF-HFP membrane electrolyte (reprinted from ref. 100 Copyright 2008, with permission from the American Chemical Society).

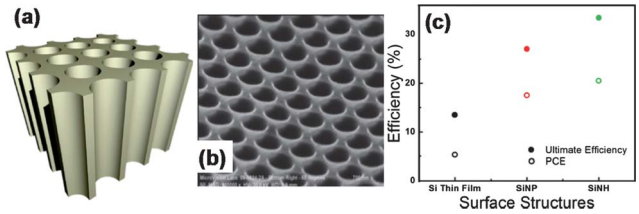

Fig. 19 (a) Schematic illustration (reprinted from ref. 104 Copyright 2010, with permission from the American Chemical Society) and (b) SEM image of a nanohole array (reprinted from ref. 105 Copyright 2011, with permission from the American Institute of Physics). (c) Power conversion efficiency (PCE) and ultimate efficiency of Si thin film solar cells with and without nanopillar (NP) and nanohole (NH) array surface textures at AM 1.5G spectrum (reprinted from ref. 106 Copyright 2011, with permission from the American Institute of Physics).

Finally, it should be mentioned that almost all of the current photovoltaic technologies shown in Fig. 3 suffer from material or resource limitations that may prevent them from being developed to a terawatt scale.[111] These constraints include, for instance, high energy input for crystalline Si cells, materials scarcity for CdTe, $CuIn_{1-x}Ga_xSe_2$ and dye-sensitized cells which use scarce elements like tellurium, indium and ruthenium, limited material production for GaAs cells, and limited silver reserve for silver electrode/contact or back reflector used in most photovoltaic devices. So, in order to reach a terawatt scale, significant technological breakthroughs are needed for cost-effective solar cells that can avoid the natural resource limitations.

Acknowledgements

This work was supported by the HKUST (Project No. DAG09/10.EG09) and HKUST Research Project Competition Grant (RPC11EG38), the National Natural Science Foundation of China (NSFC, Grant No. 11074138), Shandong Province Natural Science Foundation for Distinguished Young Scholars (Grant No. JQ201103) and the National Key Basic Research Development Program of China (973 special preliminary study plan) (Grant No. 2012CB722705).

Notes and references

1 http://www.eia.gov/.
2 M. I. Hoffert, K. Caldeira, A. K. Jain, E. F. Haites, L. D. D. Harvey, S. D. Potter, M. E. Schlesinge, S. H. Schneider, R. G. Watts, T. M. L. Wigley and D. J. Wuebbles, *Nature*, 1998, **395**, 881.
3 http://www.erec.org/media/publications/2040-scenario.html, p. 11 in *Renewable Energy Scenario to 2040*, 2004.
4 (*a*) *PV Roadmap Toward 2030*, New Energy and Industrial Technology Development Organization (NEDO), June 2004; (*b*) I. Sakata, F. Aratani, K. Ishiyama, K. Kawakami, T. Munakata, K. Uda, H. Kudo, T. Yasui, H. Mitsuyasu, Y. Takaka and K. Koizawa. *PV Roadmap Toward 2030 in Japan*. Proceedings of the 15th International Photovoltaic Science & Engineering Conference (PVSEC-15), Shanghai, China, 2005.
5 (*a*) *Research Cell Efficiency Plot for Various Photovoltaic Technologies 1976–2011. Data compiled by Lawrence Kazmerski*, National Renewable Energy Laboratory (NREL), September 2011. http://www.nrel.gov; (*b*) M. A. Green. *Third Generation Photovoltaics: Advanced Solar Energy Conversion*. Springer-Verlag , Berlin Heidelberg, 2003; pp. 1–4.
6 M. Law, L. E. Greene, J. C. Johnson, R. Saykally and P. D. Yang, *Nat. Mater.*, 2005, **4**(6), 455.
7 B. Z. Tian, X. L. Zheng, T. J. Kempa, Y. Fang, N. F. Yu, G. H. Yu, J. L. Huang and C. M. Lieber, *Nature*, 2007, **449**(7164), 885.
8 Z. Y. Fan, H. Razavi, J. W. Do, A. Moriwaki, O. Ergen, Y. L. Chueh, P. W. Leu, J. C. Ho, T. Takahashi, L. A. Reichertz, S. Neale, K. Yu, M. Wu, J. W. Ager and A. Javey, *Nat. Mater.*, 2009, **8**, 648.
9 Z. Y. Fan, D. J. Ruebusch, A. A. Rathore, R. Kapadia, O. Ergen, P. W. Leu and A. Javey, *Nano Res.*, 2009, **2**, 829.
10 J. Zhu, Z. F. Yu, S. H. Fan and Y. Cui, *Mater. Sci. Eng., R*, 2010, **70**, 330.
11 (*a*) A. I. Hochbaum and P. D. Yang, *Chem. Rev.*, 2010, **110**, 527; (*b*) K. Q. Peng and S. T. Lee, *Adv. Mater.*, 2011, **23**(2), 198; (*c*) J. Weickert, R. B. Dunbar, H. C. Hesse, W. Wiedemann and L. Schmidt-Mende, *Adv. Mater.*, 2011, **23**(16), 1810.
12 Q. F. Zhang and G. Z. Cao, *Nano Today*, 2011, **6**, 91.
13 Y. N. Xia, P. D. Yang, Y. G. Sun, Y. Y. Wu, B. Mayers, B. Gates, Y. D. Yin, F. Kim and H. Q. Yan, *Adv. Mater.*, 2003, **15**(5), 353.
14 S. V. N. T. Kuchibhatle, A. S. Karakoti, D. Bera and S. Seal, *Prog. Mater. Sci.*, 2007, **52**(5), 699.
15 Y. Z. Long, M. M. Li, C. Z. Gu, M. X. Wan, J. L. Duvail, Z. W. Liu and Z. Y. Fan, *Prog. Polym. Sci.*, 2011, **36**(10), 1415.
16 Y. F. Li, J. H. Zhang and B. Yang, *Nano Today*, 2010, **5**, 117.

17 J. L. Duvail, S. Dubois, S. Demoustier-Champagne, Y. Z. Long and L. Piraux, *Int. J. Nanotechnol.*, 2008, **5**(6/7/8), 838.
18 Z. Y. Fan, D. Dutta, C. J. Chien, H. Y. Chen, E. C. Brown, P. C. Chang and J. G. Lu, *Appl. Phys. Lett.*, 2006, **89**(21), 213110.
19 Z. M. Huang, Y. Z. Zhang, M. Kotaki and S. Ramakrishna, *Compos. Sci. Technol.*, 2003, **63**, 2223.
20 X. F. Lu, C. Wang and Y. Wei, *Small*, 2009, **5**(21), 2349.
21 M. M. Li, Y. Z. Long, D. Y. Yang, J. S. Sun, H. X. Yin, Z. L. Zhao, W. H. Kong, X. Y. Jiang and Z. Y. Fan, *J. Mater. Chem.*, 2011, **21**, 13159.
22 Z. Y. Fan, R. Kapadia, P. W. Leu, X. B. Zhang, Y. L. Chueh, K. Takei, K. Yu, A. Jamshidi, A. A. Rathore, D. J. Ruebusch, M. Wu and A. Javey, *Nano Lett.*, 2010, **10**, 3823.
23 E. Garnett and P. D. Yang, *Nano Lett.*, 2010, **10**, 1082.
24 K. Forberich, G. Dennler, M. C. Scharber, K. Hingerl, T. Fromherz and C. J. Brabec, *Thin Solid Films*, 2008, **516**, 7167.
25 G. J. Lin, K. Y. Lai, C. A. Lin, Y. L. Lai and J. H. He, *IEEE Electron Device Lett.*, 2011, **32**(8), 1104.
26 S. J. Wilson and M. C. Hutley, *J. Mod. Opt.*, 1982, **29**(7), 993.
27 C. Lin and M. L. Povinelli, *Opt. Express*, 2009, **17**, 19371.
28 L. Hu and G. Chen, *Nano Lett.*, 2007, **7**, 3249.
29 A. Chutinan and S. John, *Phys. Rev. A: At., Mol., Opt. Phys.*, 2008, **78**, 023825.
30 D. Y. Zhou and R. Biswas, *J. Appl. Phys.*, 2008, **103**(09), 093102.
31 O. L. Muskens, J. G. Rivas, R. E. Algra, E. P. A. M. Bakkers and A. Lagendijk, *Nano Lett.*, 2008, **8**(9), 2638.
32 B. M. Kayes, H. A. Atwater and N. S. Lewis, *J. Appl. Phys.*, 2005, **97**(11), 114302.
33 J. M. Spurgeon, H. A. Atwater and N. S. Lewis, *J. Phys. Chem. C*, 2008, **112**(15), 6186.
34 (*a*) W. L. Min, B. Jiang and P. Jiang, *Adv. Mater.*, 2008, **20**(20), 3914; (*b*) Y. R. Lin, K. Y. Lai, H. P. Wang and J. H. He, *Nanoscale*, 2010, **2**, 2765.
35 Y. F. Li, J. H. Zhang, S. J. Zhu, H. P. Dong, Z. H. Wang, Z. Q. Sun, J. R. Guo and B. Yang, *J. Mater. Chem.*, 2009, **19**, 1806.
36 Y. F. Li, J. H. Zhang, S. J. Zhu, H. P. Dong, F. Jia, Z. H. Wang, Z. Q. Sun, L. Zhang, Y. Li, H. B. Li, W. Q. Xu and B. Yang, *Adv. Mater.*, 2009, **21**(46), 4731.
37 H. Bao and X. L. Ruan, *Opt. Lett.*, 2010, **35**(20), 3378.
38 S. H. Baek, H. S. Jang and J. H. Kim, *Curr. Appl. Phys.*, 2011, **11**, S30.
39 R. Y. Lu and A. Lal, *Nano Lett.*, 2010, **10**, 4651.
40 Y. H. Kuang, K. H. M. van der Werf, Z. S. Houweling and R. E. I. Schropp, *Appl. Phys. Lett.*, 2011, **98**, 113111.
41 R. Peköz, O. B. Malcıoğlu and J. Y. Raty, *Phys. Rev. B: Condens. Matter Mater. Phys.*, 2011, **83**, 035317.
42 C. Colombo, M. Heiss, M. Gratzel and A. F. I. Morral, *Appl. Phys. Lett.*, 2009, **94**, 173108.
43 J. A. Czaban, D. A. Thompson and R. R. LaPierre, *Nano Lett.*, 2009, **9**, 148.
44 R. R. LaPierre, *J. Appl. Phys.*, 2011, **109**, 034311.
45 R. E. Camacho, A. R. Morgan, M. C. Flores, T. A. McLeod, V. S. Kumsomboone, B. J. Mordecai, R. Bhattacharjea, W. Tong, B. K. Wagner, J. D. Flicker, S. P. Turano and W. J. Ready, *JOM*, 2007, **59**(3), 39.
46 J. Flicker and J. Ready, *J. Appl. Phys.*, 2008, **103**(11), 113110.
47 R. Kapadia, Z. Y. Fan and A. Javey, *Appl. Phys. Lett.*, 2010, **96**(10), 103116.
48 S. Chu, D. D. Li, P. C. Chang and J. G. Lu, *Nanoscale Res. Lett.*, 2011, **6**(1), 38.
49 Y. F. Hsu, Y. Y. Xi, A. B. Djurišić and W. K. Chan, *Appl. Phys. Lett.*, 2008, **92**(13), 133507.
50 P. Charoensirithavorn, T. Sagawa, S. Hayase and S. Yoshikawa, *J. Sol. Energy Eng.*, 2011, **133**(1), 011101.
51 Q. L. Huang, L. Fang, X. Chen and M. Saleem, *J. Alloys Compd.*, 2011, **509**, 9456.
52 X. J. Feng, K. Shankar, O. K. Varghese, M. Paulose, T. J. Latempa and C. A. Grimes, *Nano Lett.*, 2008, **8**(11), 3781.
53 B. Liu and E. S. Aydil, *J. Am. Chem. Soc.*, 2009, **131**(11), 3985.
54 F. shao, J. Sun, L. Gao, S. W. Yang and J. Q. Luo, *J. Phys. Chem. C*, 2011, **115**, 1819.
55 M. Quintana, T. Edvinsson, A. Hagfeldt and G. Boschloo, *J. Phys. Chem. C*, 2007, **111**(2), 1035.
56 Y. G. Wei, C. Xu, S. Xu, C. Li, W. Z. Wu and Z. L. Wang, *Nano Lett.*, 2010, **10**, 2092.
57 J. M. Macák, H. Tsuchiya, Ghicov and P. Schmuki, *Electrochem. Commun.*, 2005, **7**(11), 1133.
58 G. K. Mor, K. Shankar, M. Paulose, O. K. Varghese and C. A. Grimes, *Nano Lett.*, 2006, **6**(2), 215.
59 M. Paulose, K. Shankar, O. K. Varghese, G. K. Mor, B. Hardin and C. A. Grimes, *Nanotechnology*, 2006, **17**(5), 1446.
60 J. H. Park, T. W. Lee and M. G. Kang, *Chem. Commun.*, 2008, 2867.
61 J. Bandara, K. Shankar, J. Basham, H. Wietasch, M. Paulose, O. K. Varghese, C. A. Grimes and M. Thelakkat, *Eur. Phys. J.: Appl. Phys.*, 2011, **53**, 20601.
62 J. B. Han, F. R. Fan, C. Xu, S. S. Lin, M. Wei, X. Duan and Z. L. Wang, *Nanotechnology*, 2010, **21**(40), 405203.
63 A. B. F. Martinson, J. W. Elam, J. T. Hupp and M. J. Pellin, *Nano Lett.*, 2007, **7**(8), 2183.
64 A. B. F. Martinson, M. S. Goes, F. Fabregat-Santiago, J. Bisquert, M. J. Pellin and J. T. Hupp, *J. Phys. Chem. A*, 2009, **113**(16), 4015.
65 C. H. Ku and J. J. Wu, *Appl. Phys. Lett.*, 2007, **91**(09), 093117.
66 Y. Q. Wang, Y. M. Sun and K. Li, *Mater. Lett.*, 2009, **63**(12), 1102.
67 X. Y. Gan, X. M Li, X. D. Gao, F. W. Zhuge and W. D. Yu, *Thin Solid Films*, 2010, **518**(17), 4809.
68 S. Yodyingyong, Q. F. Zhang, K. Park, C. S. Dandeneau, X. Y. Zhou, D. Triampo and G. Z. Cao, *Appl. Phys. Lett.*, 2010, **96**(07), 073115.
69 Y. Alivov and Z. Y. Fan, *Appl. Phys. Lett.*, 2009, **95**(06), 063504.
70 M. Law, L. E. Greene, A. Radenovic, T. Kuykendall, J. Liphardt and P. D. Yang, *J. Phys. Chem. B*, 2006, **110**(45), 22652.
71 S. Gubbala, V. Chakrapani, V. Kumar and M. K. Sunkara, *Adv. Funct. Mater.*, 2008, **18**(16), 2411.
72 J. Chung, J. Myoung, J. Oh and S. Lim, *J. Phys. Chem. C*, 2010, **114**(49), 21360.
73 (*a*) J. H. Bang and P. V. Kamat, *Adv. Funct. Mater.*, 2010, **20**(12), 1970; (*b*) J. Xu, X. Yang, H. K. Wang, X. Chen, C. Y. Luan, Z. X. Xu, Z. Z. Lu, V. A. L. Roy, W. J. Zhang and C. S. Lee, *Nano Lett.*, 2011, **11**(10), 4138.
74 W. Chen, H. F. Zhang, I. M. Hsing and S. H. Yang, *Electrochem. Commun.*, 2009, **11**(5), 1057.
75 W. Chen and S. H. Yang, *Front. Optoelectron. China*, 2011, **4**(1), 24.
76 H. M. Cheng, W. H. Chiu, C. H. Lee, S. Y. Tsai and W. F. Hsieh, *J. Phys. Chem. C*, 2008, **112**(42), 16359.
77 F. Sauvage, F. D. Fonzo, A. L. Bassi, C. S. Casari, V. Russo, G. Divitini, C. Ducati, C. E. Bottani, P. Comte and M. Graetzel, *Nano Lett.*, 2010, **10**(7), 2562.
78 S. H. Ko, D. Lee, H. W. Kang, K. H. Nam, J. Y. Yeo, S. J. Hong, C. P. Grigoropoulos and H. J. Sung, *Nano Lett.*, 2011, **11**, 666.
79 J. B. Baxter and E. S. Aydil, *Sol. Energy Mater. Sol. Cells*, 2006, **90**(5), 607.
80 C. Y. Jiang, X. W. Sun, G. Q. Lo, D. L. Kwong and J. X. Wang, *Appl. Phys. Lett.*, 2007, **90**(26), 263501.
81 Q. F. Zhang, T. R. Chou, B. Russo, S. A. Jenekhe and G. Z. Cao, *Angew. Chem., Int. Ed.*, 2008, **47**(13), 2402.
82 C. S. Rustomji, C. J. Frandsen, S. Jin and M. J. Tauber, *J. Phys. Chem. B*, 2010, **114**(45), 14537.
83 Y. J. Kim, M. H. Lee, H. J. Kim, G. Lim, Y. S. Choi, N. G. Park, K. Kim and W. I. Lee, *Adv. Mater.*, 2009, **21**(36), 3668.
84 S. C. Yang, D. J. Yang, J. Kim, J. M. Hong, H. G. Kim and I. D. Kim, *Adv. Mater.*, 2008, **20**, 1059.
85 W. Chen, Y. C. Qiu, Y. C. Zhong, K. S. Wong and S. H. Yang, *J. Phys. Chem. A*, 2010, **114**(9), 3127.
86 C. T. Wu, W. P. Liao and J. J. Wu, *J. Mater. Chem.*, 2011, **21**(9), 2871.
87 W. P. Liao and J. J. Wu, *J. Mater. Chem.*, 2011, **21**(25), 9255.
88 M. J. Laudenslager, R. H. Scheffler and W. M. Sigmund, *Pure Appl. Chem.*, 2010, **82**(11), 2137.
89 Z. X. Dong, S. J. Kennedy and Y. Q. Wu, *J. Power Sources*, 2011, **196**, 4886.
90 S. Chuangchote, T. Sagawa and S. Yoshikawa, *Appl. Phys. Lett.*, 2008, **93**(03), 033310.
91 M. Y. Song, Y. R. Ahn, S. M. Jo, D. Y. Kim and J. P. Ahn, *Appl. Phys. Lett.*, 2005, **87**(11), 113113.
92 I. D. Kim, J. M. Hong, B. H. Lee, D. Y. Kim, E. K. Jeon, D. K. Choi and D. J. Yang, *Appl. Phys. Lett.*, 2007, **91**(16), 163109.
93 H. S. Shim, S. I. Na, S. H. Nam, H. J. Ahn, H. J. Kim, D. Y. Kim and W. B. Kim, *Appl. Phys. Lett.*, 2008, **92**(18), 183107.
94 S. J. Wu, Q. D. Tai and F. Yan, *J. Phys. Chem. C*, 2010, **114**(13), 6197.
95 Q. D. Tai, X. Z. Zhao and F. Yan, *J. Mater. Chem.*, 2010, **20**, 7366.

96 T. Krishnamoorthy, V. Thavasi, G. M. Subodh and S. Ramakrishna, *Energy Environ. Sci.*, 2011, **4**, 2807.
97 K. Fujihara, A. Kumar, R. Jose, S. Ramakrishna and S. Uchida, *Nanotechnology*, 2007, **18**(36), 365709.
98 P. Joshi, L. F. Zhang, D. Davoux, Z. T. Zhu, D. Galipeau, H. Fong and Q. Q. Qiao, *Energy Environ. Sci.*, 2010, **3**(10), 1507.
99 Y. Zhao, J. Zhai, T. Wei, L. Jiang and D. B. Zhu, *J. Mater. Chem.*, 2007, **17**, 5084.
100 A. R. S. Priya, A. Subramania, Y. S. Jung and K. J. Kim, *Langmuir*, 2008, **24**(17), 9816.
101 J. U. Kim, S. H. Park, H. J. Choi, W. K. Lee and M. R. Kim, *Sol. Energy Mater. Sol. Cells*, 2009, **93**, 803.
102 J. E. Allen, E. R. Hemesath, D. E. Perea, J. L. Lensch-Falk, Z. Y. Li, F. Yin, M. H. Gass, P. Wang, A. L. Bleloch, R. E. Palmer and L. J. Lauhon, *Nat. Nanotechnol.*, 2008, **3**(3), 168.
103 Y. P. Dan, K. Seo, K. Takei, J. H. Meza, A. Javey and K. B. Crozier, *Nano Lett.*, 2011, **11**, 2527.
104 S. E. Han and G. Chen, *Nano Lett.*, 2010, **10**, 1012.
105 J. Bhattacharya, N. Chakravarty, S. Pattnaik, W. D. Slafer, R. Biswas and V. L. Dalal, *Appl. Phys. Lett.*, 2011, **99**(13), 131114.
106 F. Wang, H. Y. Yu, J. S. Li, S. Wong, X. W. Sun, X. C. Wang and H. Y. Zheng, *J. Appl. Phys.*, 2011, **109**(08), 084306.
107 M. Vanecek, O. Babchenko, A. Purkrt, J. Holovsky, N. Neykova, A. Poruba, Z. Remes, J. Meier and U. Kroll, *Appl. Phys. Lett.*, 2011, **98**(16), 163503.
108 J. Gjessing, A. S. SudbØ and E. S. Marstein, *J. Appl. Phys.*, 2011, **110**(03), 033104.
109 W. Wang, S. Wu, R. J. Knize, K. Reinhardt, Y. Lu and S. Chen, *Opt. Express*, 2012, **20**(4), 3733.
110 R. Yu, K. L. Ching, Q. Lin, S. F. Leung, D. Arcrossito and Z. Fan, *ACS Nano*, 2011, **5**(11), 9291.
111 C. S. Tao, J. C. Jiang and M. Tao, *Sol. Energy Mater. Sol. Cells*, 2011, **95**, 3176.

